THE EXPERIMENTAL ANALYSIS OF LOCAL HEAT AND MASS TRANSFER DATA FOR VERTICAL FALLING FILM ABSORPTION

William A. Miller, Ph.D., Research Engineer
Oak Ridge National Laboratory'
Oak Ridge, TN 37831

Majid Keyhani, Ph.D., Professor
Mechanical & Aerospace Engineering and Engineering Science Department
University of Tennessee, Knoxville

ABSTRACT

In pure heat transfer, specifications of effectiveness, fluid properties, and flows enable calculation of the heat exchanger area. In the case of falling film absorption, a simultaneous heat and mass transfer governs the performance of the absorber. The exchange of mass across the liquid-vapor interface involves the generation of heat. The heat effects associated with the mass exchange increase the temperature, which affects the equilibrium state of the pressure and composition and in turn affects the mass. The falling film flow rate coupled to the physical properties of kinematic viscosity and surface tension govern the flow regime of a vertical falling film. Wavy-laminar, roll-wave laminar, and turbulent flows will develop convective contributions that can enhance the transfer of mass into the film.

The combined interaction of all these factors makes the absorption process very difficult to analyze and predict. A study of simultaneous heat and mass transfer was therefore conducted on a vertical falling film absorber to better understand the mechanisms driving the heat and mass transfer processes. Falling films are characteristically unstable, and a wavy-laminar flow was observed during the experimental study. The wavy flow further complicates the problem; therefore, only limited information is known about the temperature and concentration profiles along the length of the absorber that describe the local heat and mass transfer rates.

Hence, this study presents much-needed experimental data on the heat and mass transfer processes in the absence of heat and mass transfer additive. Absorption experiments were conducted in a mini-absorber test stand at various falling film flow rates, at various absorber pressures, and with various compositions of the binary salt solution. Thermographic phosphors were successfully used to measure the temperature profile along the length of the absorber test tube. These measures of the local variations in temperature enabled calculation of the bulk concentration along the length of the absorber. The bulk concentration varied linearly, from which one may infer that the concentration gradient in the direction of flow is approximately constant. The implication is that the mass flux, and therefore the absorber load, can be solved for by using a constant flux approximation.

INTRODUCTION

Absorption is the assimilation of one or more constituents of a gas or vapor into a liquid by mass transfer. Absorption chillers use falling films of aqueous LiBr that absorb water vapor in an absorber. The absorber is the largest of the heat exchangers and is the heart of a thermally activated chiller. Its performance is paramount to the overall performance of the machine. The more refrigerant absorbed per unit of absorbent, the greater the refrigerant mass flow rate available for the evaporator, which in turn increases the comfort cooling capacity of the chiller. Hence, improvements in system performance are integrally tied to a fundamental understanding of falling film hydrodynamics and the simultaneous heat and mass transfer processes occurring within the absorber. A small amount of heat and mass transfer additive is used to enhance performance, and sizing is based on an empirical approach, which can be costly. HVAC manufacturers view the serendipitous discovery of the additive effect as a cost-effective means of achieving a twofold boost in performance through chemical rather than mechanical enhancement. Hence, the

†Managed by Lockheed Martin Energy Research Corporation under Contract DE-AC05-96OR22464 for the U.S. Department of Energy.

NOMENCLATURE

SYMBOL	DESCRIPTIVE	SI UNITS
C_a	Concentration of absorbate	g-mole H_2O/cc soln
CP	Specific heat at constant pressure	kJ/kg· K
DAB	Diffusivity of *a* through *b*	m^2/s
h_m	Local liquid-side mass transfer coefficient	m/s
h	Local heat transfer coefficient	J/ m^2 ·K · s
i_{fg}	Latent heat of water vapor	kJ/Kg
k	Thermal conductivity	J/m ·K · s
$\dot{m}$	Mass flow rate	kg/s
$\dot{m}'_v$	Absorbatc mass flow rate per unit length	kg / m ·s
4	Heat transfer rate	J/s
q'	Heat transfer per unit length	J/ m· s
R, r	Pipe radius	m
P_v	Absorber pressure	kPa
T	Temperature	°C
$\overline{U}$	Average falling film velocity	m/s
u	Local streamwise velocity, in *x* direction	m/s
x	Coordinate in direction of flow	m
y	Coordinatc normal to direction of flow	m
A	Average film thickness	m
η'	Molecular weight of water	g/g-moles
ν	Kinematic viscosity	m^2/s
ρ	Density	g/cc
X	Mass fraction	kg LiBr / kg soln

Subscripts and Superscripts

CL	Coolant
f	Film
ı	Inside diameter or inside radius
o	Outside diameter or outside radius
p	Pipe
v	Absorbate vapor
wall	Tube wall
–	Bulk or average value
*	Liquid-vapor interface

Dimensionless Groups

Re	Reynolds number	$4\overline{U}\Delta/\nu$
SC	Schmidt number	ν/D_{ab}

issues of falling film hydrodynamics, thermodynamic and transport properties, the magnitude of the heat effects and composition at the vapor-liquid interface. and heat and mass transfer from the vapor-liquid interface were of secondary concern until the recent resurgence of absorption technology. A better understanding of the fundamental issues governing the absorption process must precede the advancement of design.

Almost all chillers use a horizontal rather than a vertical tube bundle in the absorber. HVAC manufacturers consider the horizontal configuration superior to the vertical because it better mixes the absorbate into the film. The droplets form at the bottom of a horizontal tube and splash onto the lower tubes within the bundle. The intimate contact between the droplets and the vapor and the subsequent splashing action is believed to enhance performance; however, Burdukov et al. (1980) experimentally proved similar performance for vertical and horizontal absorbers when tested with no heat and mass transfer additive. Bicrmann (1980) experimentally found identical performance for both absorber configurations when tested with heat and mass transfer additive. The hydrodynamics of vertical tube absorbers arc not clouded with questions regarding the effect of droplet formation and subsequent splashing onto the lower tubes. Therefore, the vertical tube is better suited for both experimental and analytical studies of falling film hydrodynamics and the coupled heat and mass transfer processes occurring within the absorber.

The absorption of water vapor into a falling film of aqueous LiBr is affected by several factors:

- The magnitudes of thermal and mass diffusivities in part regulate the transfer of water from the vapor-liquid interface into the bulk of the film.
- Film flow rate coupled to the physical properties of kinematic viscosity and surface tension governs the flow regime of the falling film.
- Wavy-laminar, roll-wave laminar, and turbulent flows will develop convective contributions that can enhance the transfer of mass into the film.
- The magnitude of the heat release and the pressure-temperature-concentration relationship for aqueous LiBr govern the rate at which mass is absorbed into the film.
- Inert gases such as air can blanket the interface and will retard absorption by elevating the partial pressure at the interface.
- The rate of heat transfer to the coolant affects the film temperature and is probably the major player in controlling the absorption process.

The combined interaction of all these factors makes the process very difficult to analyze. While some experimental data are available, all experiments in the literature to date have been conducted at LiBr concentrations ranging from 0.30 to 0.60 mass fraction. No literature data are readily available at the design operating conditions—LiBr concentrations of 0.62 and 0.64 mass fraction and absorber pressure of 0.7 and I kPa (see Miller and Keyhani, 1999).

In addition, little is known about temperature and concentration profiles along the length of the absorber, which are indicative of local heat and mass transfer. The key for computing these local transport rates is the actual film temperature and concentration at the liquid-vapor interface. These measures continue to elude researchers but are important for understanding on a local as well as a global scale the heat effects at the interface, the heat transfer from the interface, and the mass transfer onto and through the interface.

Hence, experimental work was conducted to better understand the first-principle concepts of falling-film absorption with no heat and mass transfer additive. The driving mechanism causing enhancement with heat and mass transfer additive is a study in itself. Further, the chemical mechanism is very difficult to determine because of the dynamic complexities and the dearth of experimental data.

EXPERIMENTAL FACILITY

The experimental facility consisted of a falling-film flow loop, a heat and mass transfer test stand, and a data acquisition system. The flow loop was used to characterize the different flow regimes of a falling film and to measure the salient features of the flow. A heat and mass transfer test stand was used for testing a single stainless steel absorber tube of 0.01905-m outside diameter (OD) and I ,524-m length. A unique feature of this stand is its ability to operate continuously and support testing of LiBr brine at a mass fraction of 0.62, the design conditions for absorption chillers. Mosl heat and mass transfer test stands support testing only in batch mode and cannot easily operate without crystallizing the hrine at 0.62 mass fraction.

Miller (1998) describes the operating and testing procedures and presents details of the flow loop and the heat and mass transfer test stand as well as the salient features of the instrumentation used to monitor and collect data.

Heat and Mass Transfer Test Stand

The heat and mass transfer test stand is shown schematically in Fig. 1. For testing purposes, the vertical absorber receives vapor directly from a boiler; if it were integrated into the refrigerant circuit of a chiller, it would receive vapor from an evaporator. The vertical mini-absorber test section is made of standard Pyrex glass pipe 2. I m long with an inside diameter of 0. 15 m. Stainless steel end plates are bolted to the conical glass ends of the vessel using cast iron flanges. Coolant flow is countercurrent to the falling film and supports the coupled heat and mass transfer process as the falling film of strong solution absorbs water vapor. A dispenser and catch basin are made of 304L stainless steel; both are attached directly to the test tube. The dispenser uniformly distributes the strong solution onto the test tube.

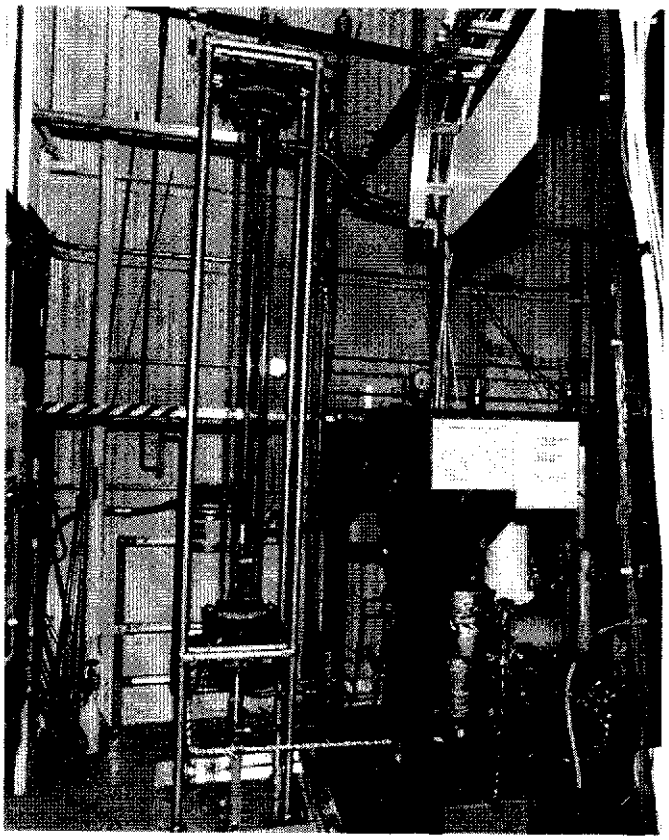

Fig. 1. Mini-absorber test section.

A simple but crucial feature of the dispenser is its design, which allows the entering strong solution to equilibrate. Holes were drilled atop the cup and a screen was inserted into the entering strong solution line lo help spray the solution into the cup (Fig. 2). Exposing the strong solution as a spray caused it to equilibrate to the pressure of the ambient vapor within the absorber. Hence, the thermodynamic state point of the brine is known at the start of the simultaneous **heat and mass transfer** process.

Instrumentation

The test stand is instrumented at various locations for the measurement of temperature, pressure, density, flows, and boiler **power.** The test tube was also instrumented to measure the temperature profiles of the coolant, the wall, and the falling film along the running length of the absorber tube. A probe 1.8 m long and with a 6.35-mm OD was inserted inside the absorber test tube for measuring the local bulk temperature of the coolant along its flow path. The probe also helped enhance the turbulent flow of the coolant. The probe has a stainless steel sheath and is composed of ten Type T thermocouples spaced about 0.15 m apart Resistance temperature detectors (RTDs) were selected for measuring wall temperatures because the sensor measures an average temperature over its exposed length. The falling film flow is not symmetric

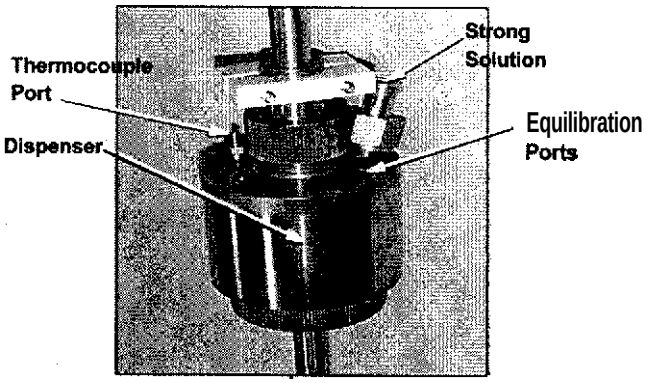

Fig. 2. The dispenser used in the flow loop and in the mini-absorber test section.

because of the wavy flow, and an average perimeter measurement is more representative of the wall's temperature than is a point measurement made with a thermocouple.

A non-intrusive technique developed jointly at Los Alamos National Laboratory and Oak Ridge National Laboratory was used to measure the falling film temperature profile. This approach **involves seeding the** LiBr brine with thermographic phosphors and measuring the fluorescent decay rate of the phosphor when a pulsed nitrogen laser excites the solution. The phosphor, lanthanum oxysulfide doped with europium (La_2O_2S:Eu), has an emission spectrum consisting of many sharply defined spectral lines, some of which are a strong function of temperature (Allison et al., 1989). The experimental setup is illustrated in Fig. 3. The nitrogen laser produces an excitation beam with a wavelength of 337 nm and a pulse duration of about 20 ns. The ultraviolet irradiation excites the thermographic phosphors and causes them to emit many sharply detined visible spectral lines. A photomultiplier tube detects the radiation emitted from the phosphor and outputs data to a programmable storage oscilloscope for data acquisition and measurement of the decay rate of the phosphors (Fig. 3). As a caveat, the velocity of the falling film was about 0.5 m/s, and the phosphor particles were within a 6-mm excitation region on the film for about 0.02 s; the fluorescent decay of the particles was therefore easily detected during the 20-ns pulse.

LOCAL HEAT AND MASS TRANSFER EXPERIMENTS

Modern-day absorption chillers operate in the wavy-laminar flow regime. The flow enters as a smooth laminar tlow but quickly transitions into a wavy flow. For vertical absorbers, the waves grow in length and amplitude and are identifiable as roll waves. Roll waves were observed during our testing. At the lowest flow of 0.014 kg/s, the inception of short, small-amplitude waves was seen about 0.2 m from the inlet. The short waves transition into longer roll-waves whose length and amplitude arc at least twice those of the short waves.

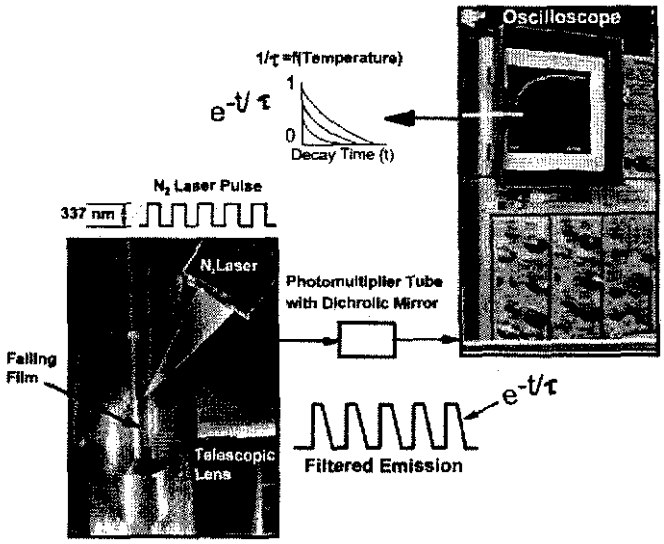

Fig. 3. Non-intrusive **film temperature measurements were made using thermographic phosphors.**

The simultaneous release of heat further complicates the analysis of mass transfer in wavy films. The heat effects at the interface, the heat transfer from the interface, and the mass transfer onto and through the interface are all affected by variations of the roll waves. As a further complication, the composition of a binary mixture cannot he determined solely on the basis of temperature. Computing these local variations in heat and mass transfer rates requires a determination of the film temperature and concentration. Conventional film temperature sensors would disrupt the normal flow patterns in a thin falling film.

The test tube was instrumented internally to measure the axial temperature profile of the coolant. The charge of LiBr brine was doped with a lanthanum oxysultide phosphor to support the non-intrusive measure of the interface temperature. Testing was conducted at an entering solution concentration of 60 wt%. The Re number of the falling film was fixed at about 290, and the coolant temperature was controlled to 35°C. Absorber pressure war controlled throughout all testing at 1.3 kPa. For these operating conditions, the measures of the coolant and interface temperatures are plotted in Fig. 4. The symbols in Fig. 4 represent the measured data, and the lines are exponential curve fits of the form shown in Eq. 1.

The vertical bars represent the error in the data. The coolant probe was calibrated and checked in situ; its measurement error was ±0.15°C. Preliminary testing with thermographic phosphors showed an error of about ± 0.5°C; however, in the mini-absorber, we repeated several measurements at a given station to better estimate the actual error. Results showed the interface temperatures to be accurate to about ±1.5°C. Despite this large error, the trends are very useful for understanding on an overall

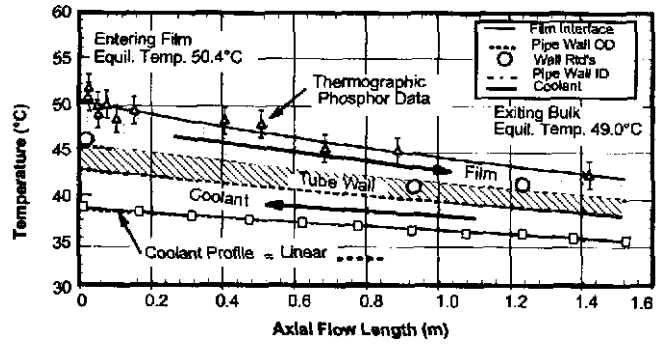

Fig. 4. Thermographic phosphor and coolant temperature profiles measured along the running length of the falling film.

scale the coupled heat and mass transfer processes. Surprisingly, the curve fit through the coolant data shows an almost linear temperature gain over the full length of the absorber.

Grossman and Alefeld (1 996) also discovered this result. Grossman inserted ten thermocouples into the bore of a stainless steel test tube to measure the coolant temperature distribution. Unfortunately, the thermocouples were delicate and malfunctioned after a few tests. While they were operable, however, Grossman observed the profile to be slightly exponential but rather flat and approximately linear. In fact, the solid coolant curve in Fig. 4 is exponential in form (Eq. 1), while the dashed curve is a linear tit to the measured data. Close inspection of Fig. 4 shows a similar slight exponential deviation for the last three coolant temperatures (at stations near the inlet of falling film). What is surprising, however, is the minimal effect seen on the coolant profile near **the film** inlet, where absorption heat flows are the largest.

A reduction scheme was formulated to quantify the local concentration and mass absorbed along the length of the absorber. The coolant and interface temperature data (Fig. 4) were fit to exponential profiles of the form shown in Eq. 1:

$$T(x) = a + be^{(-x/c)} . \qquad (1)$$

The coefficients are shown in Table 1

Table 1. Regression constants for the temperature profiles in Eq. 1

	a	*b*	*c*	R^2
Coolant	28.450	10.299	3.61	0.999
Film interface	33.302	16.925	2.21 I	0.872

An energy balance is set up for the control volume shown in Fig. 5. The energy balance expresses the local heat flow to the coolant from the film:

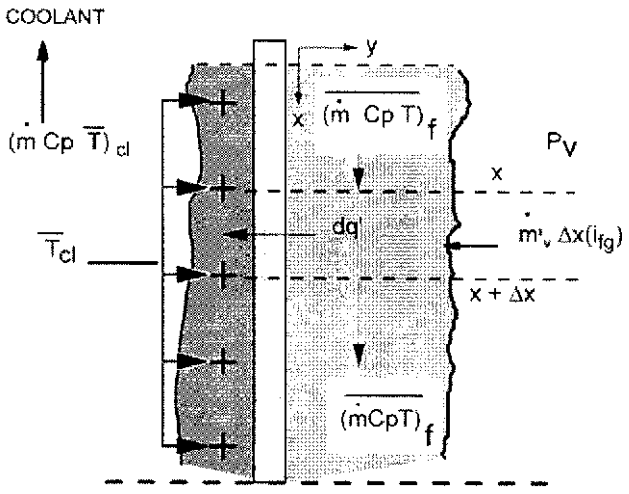

Fig. 5. Differential element for the vertical falling film absorber with counterflow coolant.

$$dq' = \left(\dot{m}C_p\right)_{CL} \frac{d\overline{T}_{CL}}{dx}. \qquad (2)$$

The differential heat flow, expressed as kJ/m·s, is calculated from the coolant side measurements by taking the gradient of Eq. 1 at a given location, x. Starting at the solution inlet, the local balance is incremented by Δx, and the gradient $d\overline{T}_{CL}/dx$, is substituted into Eq. 2 for the local heat flow. Then, given the water-side convective coefficient, the inside wall temperature profile is calculated from a first law balance:

$$T_{wall_i} = \overline{T}_{CL} + \frac{dq'}{(2\pi R_i)h_{CL}} \qquad (3)$$

The profile on the outer wall, based on conduction through the tube material, becomes

$$T_{wall_o} = T_{wall_i} + \frac{\left[\ln\left(R_O/R_i\right)\right]dq'}{2\pi k_p}. \qquad (4)$$

These calculated wall temperatures are **shown in** Fig. 4 along with measured RTD wall temperatures. The calculated and measured RTD temperatures are within 0.3°C, which substantiates the accuracy of the calculated wall profiles. By including both the coolant and film in the control volume shown in Fig. 5, the energy balance for the small element Δx becomes

$$\left(\dot{m}C_pT\right)_x + \dot{m}'_v i_{fg}\Delta x = \left(\dot{m}C_pT\right)_{x+\Delta x} + dq'\Delta x. \qquad (5)$$

Taking the limit of Eq. 5 as $\Delta x \to 0$ and substituting Eq. 2 for dq' yields an expression for the local mass absorbed per unit length.

$$\dot{m}'_v = \left[\frac{\left(\dot{m}C_p\right)_f}{i_{fg}}\right]\frac{d\overline{T}_f}{dx} + \frac{dq'}{i_{fg}} \qquad (6)$$

A water balance for the absorbate within the film side control volume of Fig. 5 yields

$$\left(\frac{\dot{m}}{\rho}\right)_f \eta'\overline{C}_a\Big|_x + \dot{m}'_v\Delta x = \left(\frac{\dot{m}}{\rho}\right)_f \eta'\overline{C}_a\Big|_{x+\Delta x}. \qquad (7)$$

Again taking the limit of Eq. 7 as $\Delta x \to 0$ yields the continuity expression

$$\dot{m}'_v = \left(\frac{\dot{m}}{\rho}\right)_f \eta'\frac{d\overline{C}_a}{dx} \qquad (8)$$

The concentration is derived from Eq. 8 and can be used to march down the tube for calculation of the local bulk profile, which is expressed as a bulk water concentration:

$$\overline{C}_a = \frac{\dot{m}'_v\Delta x}{\eta'\left(\dot{m}/\rho\right)} \qquad (9)$$

This equation can also **be** expressed in terms of the solute:

$$\overline{X}_f = 1 - \frac{\dot{m}'_v\Delta x}{\dot{m}_f}. \qquad (10)$$

The differential mass absorbed is expressed in units of kg/m·s. The energy balance of Eq. 6 is dependent on the gradient of the bulk temperature in the film with respect to the tube length. Thermographic phosphor measurements are considered interface temperatures, and a local bulk temperature was needed as input to Eq. 6. The roll waves are a determining factor in assuming that the particles were dispersed more on the surface of the film than in its bulk. The hydrodynamic sweeping action of each successive roll wave (Brauner and Maron 1982) keeps the thermographic phosphor particles near the free surface of the falling film. In the substrate, Chu and Duklcr (1974) measured a substrate thickness of about 1000 μm for a Re number of 1000. The thermographic particles are about 10 μm thick. Therefore, about one-tenth of the substrate is composed of the phosphors. Further, the thermographic phosphor data yielded a temperature very close to the equilibrium temperature reached by the absorbent near the absorber inlet when first introduced to the ambient vapor as a falling film (Fig. 4).

The correspondence is very promising and helps substantiate the accuracy of the interface measurements. Use of the definition for bulk temperature,

$$\dot{m}C_p\overline{T}_f = \rho C_p \int_a u(y)T(y)2\pi R_o dy \quad . \qquad (11)$$

allows a parabolic velocity profile and a linear temperature profile to be substituted into Eq. 11 to derive an expression for the local bulk temperature. The film is very thin, about 0.48 mm, and is assumed to be conduction-dominated. The linear temperature profile through the film thickness is therefore

$$T(y) = T_{wall_o} + \left(\frac{T^* - T_{wall_o}}{\Delta}\right)y, \qquad (12)$$

which yields the following simple relation for the hulk temperature:

$$\overline{T}_f = \frac{5}{8}T^* + \frac{3}{8}T_{wall_o} \cdot \qquad (13)$$

THE CALCULATION PROCEDURE

To start the calculation procedure, the concentration and temperature are initialitcd to the equilibrium condition observed at the absorber inlet. The local heat flow per unit length is calculated by Eq. 2, and the wall temperature profiles are evaluated using Eqs. 3 and 4. The bulk temperature profile is then calculated and used in Eq. 6 to calculate the local mass absorbed per unit length of the absorber. By use of the absorbate water balance of Eqs. 9 and 10, the bulk concentration is determined within the Δx increment. Data calculated in a Δx increment is stored, x is incremented by Δx, and the previous values are used as entering conditions for the next increment. The procedure marches forward until the x location matches the absorber length of 1.524 tn.

Local values are summed to determine an overall calculated load and mass absorbed. The summation for mass is simply

$$\dot{m}_v = \sum_{j=0}^{N} \dot{m}'_{v_j}(\Delta x_j), \qquad (14)$$

For the absorber load, the summation becomes

$$q = \sum_{i=0}^{N} dq'_j(\Delta x_j) \qquad (15)$$

Results, including the calculated bulk concentration and temperature, were compared to the experimental data measured at the absorber exit to validate the numerical procedure (Table 2). The procedure validates well, with the mass absorbed within 8.5% of experiment. The numerical values of load and of mass absorbed were slightly over the predictions for the experiment and are physically consistent, because load and mass absorbed are directly proportional. The bulk mass fraction, X_{ex}, is in excellent agreement, while the error in temperature is in part attributable to the error in the interface temperature measurement.

Table 2. Accuracy of the numerical data reduction procedure

Value	Experiment	Numerical	Error (%)
Load (W), coolant-side	936.5	Y56.3	2.12
Load(W), film-side	1087.7	1124.4	3.37
$\dot{m}_v$, kg/s	2.64×10^{-4}	2.866×10^{-4}	8.54
X_{ex}, wt% LiBr	59.05	59.0	-0.094
T_{ex}, °C	44.4	41.0	-7.6

CONCENTRATION PROFILE AND LOCAL TRANSFER RATES

The bulk concentration profile (wt% LiBr) is plotted in Fig. 6 for the present study. Also included in Fig. 6 are the independent data by Burdukov ct al. (1980) and Grossman and Alefeld (1996). Table 3 shows the test conditions for each of the studies. Grossman and Alcfeld inserted a helically wound wire into the bore of the absorber tube to promote turbulence in the coolant although the Re number for the coolant was low, at 4500. Burdukov et al. tested at a Re number of about 60,000 to study the absorption problem with constant wall temperature. Burdukov et al. used a traversing sampler to measure the local bulk concentration of LiBr. Grossman and Alefeld had a movable cup. Hence, both of these data sets, plotted in Fig. 6, are actual measures of the local bulk concentration.

The authors' results and the results of these two studies are very eye-opening because they all display linear trends with tube length. The slope of the trends in bulk concentration varies between studies because of the strength of the coolant Rc number. Burdukov et al. tested at a coolant Re number of 60,000, while the present authors and Grossman and Alefeld tested at Re numbers of 6,000 and 4,500, respectively. The mass absorbed is a direct function of the bulk concentration gradient, $d\overline{C}_a/dx$, which is seen in Fig. 6 to be nearly constant for the independent studies. Therefore, the mass absorbed is inferred to be constant by Eq. 8 because $d\overline{C}_a/dx$ is constant. Burdukov and associates noted that the experimental observation of a constant mass flux contradicted their analytical boundary layer model. They concluded that the theory of combined heat and mass transfer developed by Grigor'yeva and Nakoryakov (1977) needed to be refined to possibly include the mixing effect of the waves.

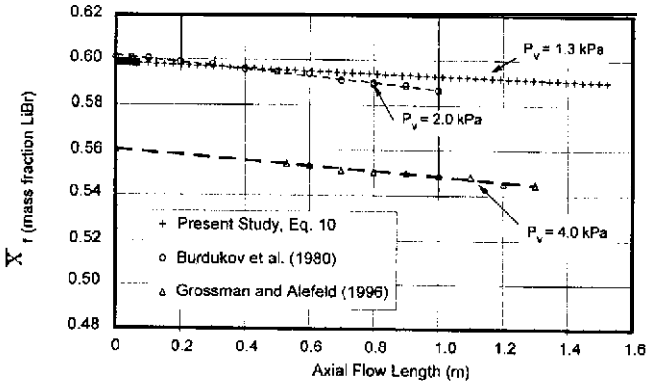

Fig. 6. Bulk concentration of the falling film for the present study compared to the independent data of Burdukov et al. (1960) and Grossman and Alefeld (1996).

Table 3. Testing conditions for the present study and two comparison studies

Parameters	Present study	Burdukov et al. 1980	Grossman and Alefeld 1996
Tube dimensions. m			
Length	I.524	1.0	1.3
OD	0.01905	0.0245	0.01905
LiBr concentration, wt%	6 0	60	56
Vapor pressure, kPa	1.3	2.03	4.0
Coolant temperaturc, °C	35	24	14
Re numbcr, falling film	290	250	280
Renumber, coolant	6,000	60,000	4,500

The experimental results reveal two very important findings. On a macro scalc, bulk film temperature and concentration profiles are roughly linear. and therefore the load and mass absorbed can he calculated using a constant flux approximation. Secondly, for Re numbers not exceeding about 400, the mass transfer is driven more by the temperature gradient across the film than it is by the normal convective forces. For the present study. thc Re number of the falling film was 290. Wasden and Dukler (1990) studied wavy flow for a Re number of 880 and reported strong convective effects across the falling film, as did Patnaik (1994). who studied a Re number of 400. Jayanti and Hewitt (1997) studied wavy flow for a Re number of 140 and reported the heat transfer as being conduction-dominated. Therefore, the convective effect within the waves does not significantly affect the process **until** the falling film transitions into the second transient turbulent-laminar regime at a Re number of about 400 (Miller, 1998). Hence, the results are consistent with the findings of Patnaik, Wasden and Dukler, and Jayanti and Hewitt.

The coupled heat and mass transfer process therefore becomes one which is mass-transfer-driven at the absorber inlet, where the solution drives to equilibrium with the vapor. The process then becomes heat-transfer-driven. As waves develop along the tube, Dukler (1976) observed the film substrate to thin, **which** causes the temperature gradient across the film to become steeper. Hence, more mass is absorbed into the thin tail section than is absorbed into the thicker wave. It may be that the interface along the wave tail is subcooled while the thicker wave is saturated at the pressure of the absorber. The thermographic phosphor data could not distinguish this subtle difference. Assuming a saturated interface, the concentration gradient across the film increases along the tube, hut the mass transfer along the tube drops because of thc brine's high diffusion resistance. Past the **entrance, the mass transfer** is driven by the heat transfer; otherwise, little if any absorption would occur. Local heat and mass transfer coefficients were calculated to substantiate the proposed concepts. The local heat transfer coefficient was calculated as

$$h = \frac{dq'}{2\pi R_o\left(T^* - T_{wall_o}\right)}, \qquad (16)$$

and the local mass transfer coefficient as

$$h_m = \frac{\dot{m}_v'}{2\pi R_o \eta'\left(C^* - \overline{C}\right)}. \qquad (17)$$

The local mass transfer coefficient was plotted against Higbie's cocfticient based on penetration:

$$\frac{h_m \Delta}{D_{ab}} = \sqrt{Re\, Sc\, \varepsilon} \qquad (18)$$

The results, plotted in Fig. 7, show that the mass transfer coefficient for thc present study exceeds that of Higbie's penetration theory [Fig. 7(a)]. However, as the axial flow length increases and fully developed flow is achieved, the two coefficients begin to converge after about 1 m. At the top of thc test tube, the flow is smooth with no waves. Yet the mass transfer coefficient is higher for the coupled heat and mass transfer of this study. The effect of the coolant enhances the mass transfer over penetration theory, and as waves develop, thc normal convective forces become more dominant. In this wavy-laminar region, however, mass is absorbed by the effect of the coolant, and enhancements by the roll waves are duc to the indirect effect of thinning the film as the waves fully develop down the tube (Miller, 1998). On the other hand, the local heat transfer coefficient is seen to increasc along the length of the tube [Fig. 7(b)], a phenomenon consistent with a thinning film. Because the film is thin (about 0.48 mm), thc heat transfer can be considered to he conduction-dominated, as alluded to by Jayanti and Hewitt (1997). Hence, thc heat transfer coefficient can he approximated as $h \approx k_f/\delta$. An increasing heat transfer coefficient therefore implies a decreasing

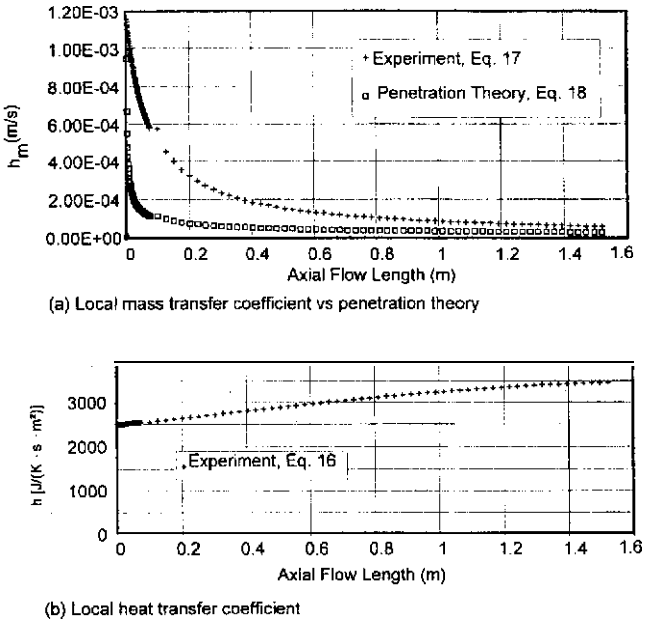

Fig. 7. Local heat and mass transport coefficients calculated for test conditions of 60 wt% LiBr, 1.3 kPa vapor pressure, 35°C coolant, and a falling film Re number of 290.

local film thickness. Conlisk (1995) analytically proved that as the inlet film thins, the mass transfer coefficient decreases and the heat transfer coefficient increases.

CONCLUSIONS

This study provides experimental data on the local heat and mass transfer processes in aqueous LiBr absorption cycle absorbers. The local bulk temperature of the absorbent was non-intrusively measured along the falling film for testing conducted at 60 wt% LiBr, with the entering coolant fixed at 35°C and the absorber pressure controlled to 1.3 kPa. A data-reduction scheme was developed to map the bulk temperature and concentration profiles over the length of the absorber. The results show that the local heat and mass transfer rates are nearly linear along the length of the absorber. The bulk concentration gradient, $d\overline{C}_a/dx$, is therefore approximately constant. The implication is that the absorber load and therefore its mass flux can he solved for using a constant flux approximation. Hence, correlation of the heat and mass transfer phenomena are no longer empirically tied to experiment. The constant flux approximation allows the correlation to be scaled to the specific length and diameter of the absorber tube.

ACKNOWLEDGMENTS

The research reported herein was sponsored by Dr. Bill Ryan of the Gas Research Institute under contracting number 5089-243-1844. The test stand was developed under the sponsorship of Ron Fiskum of DOE's Office of Building Equipment. Dr. Gershon Grossman of Technion University is commended for his willingness to share his data and his knowledge in absorption technology.

REFERENCES

Allison, S. W.; Franks, L. A.; Borella, H. M.; Lutz, S. S.; Turley, W. D.; Noel, B. W.; and Beasley, A. 1989. *Rare-Earth Phosphors for Remote Thermographic Applications.* ORNWATD-12, Oak Ridge National Laboratory. Oak Ridge, Tenn., April.

Brauner, N., and Maron, D. M. 1982. "Characteristics of Inclined Thin Films, Waviness and the Associated Mass Transfer." *Int. J. Heat Mass Transfer* 25, no. 1: 99–109.

Burdukov, A. P.; Bufetov, N. S.; Deriy, N. P.; Dorokhov, A. R.; and Kazakov, V. I. 1980. "Experimental Study of the Absorption of Water Vapor by Thin Films of Aqueous Lithium Bromide." *Heat Transfer-Soviet Res. 12, no. 3:* 118-23.

Chu, K. J., and Dukler, A. E. 1974. "Statistical Characteristics of Thin Wavy Films, Part II. Studies of the Substrate and Its Wave Structure" *AIChE J. 20, no. 4:* 695–706.

Conlisk, A. T. 1995. "Analytical Solutions for the Heat and Mass Transfer in a Falling Film Absorber." *Chem. Eng. Sci. 50,* no. 4: 65 I-60.

Dukler, A. E. 1976. "The Role of Waves in Two-Phase Flow: Some New Understandings" (Award Lecture). *Chem. Eng. Educ.* 10:108–38.

Grigor'yeva, N. I., and Nakoryakov, V. Ye. 1977. "Exact Solution of Combined Heat- and Mass-Transfer Problem during Film Absorption" (in Russian). *Inzh.-Fiz. Zh. 33, no. 5: 893-98.*

Grossman, G., and Alefeld, G. 1996. *Investigation of Heat and* Mass *Transfer* in *Absorption Heat Pumps.* GIF Report, Contract no. I-0187-100.10/9 1, Technion-Israel Institute of Technology, Haifa, Israel.

Jayanti, S., and Hewitt, G. F. 1997. "Hydrodynamics and Heat Transfer of Wavy Thin Film Flow." *Int. J. Heat Mass Transfer 40,* no. I: 179-90.

Miller, W. A. 1998. "The Experimental Analysis of Aqueous Lithium Bromide Vertical Falling Film Absorption." Ph.D. diss., University of Tennessee, Knoxville, Tenn.

Miller, W. A., and Keyhani, M. 1999. "The Correlation of Coupled Heat and Mass Transfer Experimental Data for Vertical Falling Film Absorption." *Proc. ASME Advanced Energy Systems Division--1999, vol. 39,* sess. 7B, Nashville, Tenn.

Patnaik, V. 1994. "Combined Heat **and** Mass Transfer in Wavy-Film Absorption." Ph.D. diss., Pennsylvania State Univ., University Park, Penn.

Wasdcn, F. K, and Dukler, A. E. 1990. "A Numerical Study of Mass Transfer in Free Falling Wavy Films." *AIChE J. 36, no. 9:* 1379–90.